OLIGOMERIZATION OF THE HUMAN ADENOSINE A_{2A} RECEPTOR IS DRIVEN BY THE INTRINSICALLY DISORDERED C-TERMINUS

Author Line: Khanh D. Q. Nguyen[1], Michael Vigers[2], Eric Sefah[3], Susanna Seppälä[2], Jennifer P. Hoover[1], Nicole S. Schonenbach[2], Blake Mertz[3], Michelle A. O'Malley[*,2], Songi Han[*,1,2].

Author Affiliations:

[1]Department of Chemistry and Biochemistry, University of California – Santa Barbara, CA 93106
[2]Department of Chemical Engineering, University of California – Santa Barbara, CA 93106
[3]C. Eugene Bennett Department of Chemistry, West Virginia University, 217 Clark Hall, Morgantown, WV 26506

Corresponding Authors:

- **Songi Han –** Santa Barbara, CA 93106; (805) 893-4858; songi@chem.ucsb.edu
- **Michelle A. O'Malley –** Santa Barbara, CA 93106; (805) 893-4769; momalley@engineering.ucsb.edu

Classifications: Biological Sciences – Biophysics and Computational Biology

Keywords: G protein-coupled receptors, oligomerization, intrinsically disordered protein, C-terminus, depletion interactions, size-exclusion chromatography, molecular dynamics simulations.

SIGNIFICANCE

G protein-coupled receptors (GPCRs) are important drug targets in medicine. While it is widely known that these receptors can form oligomers with unique functional consequences, the driving factor of receptor oligomerization remains unclear. The intrinsically disordered C-terminus of GPCRs is often thought to play no major role in receptor function and is thus usually removed to simplify biophysical studies. Using the human adenosine A_{2A} receptor as a model GPCR, we find instead that its C-terminus drives oligomer formation via an intricate network of interactions. This finding suggests that the distinct properties associated with GPCR oligomerization may prevail only when the C-terminus is present.

ABSTRACT

G protein-coupled receptors (GPCRs) have long been shown to exist as oligomers with functional properties distinct from those of the monomeric counterparts, but the driving factors of GPCR oligomerization remain relatively unexplored. In this study, we focus on the human adenosine A_{2A} receptor ($A_{2A}R$), a model GPCR that forms oligomers both *in vitro* and *in vivo*. Combining experimental and computational approaches, we discover that the intrinsically disordered C-terminus of $A_{2A}R$ drives the homo-oligomerization of the receptor. The formation of $A_{2A}R$ oligomers declines progressively and systematically with the shortening of the C-terminus. Multiple interaction sites and types are responsible for $A_{2A}R$ oligomerization, including disulfide linkages, hydrogen bonds, electrostatic interactions, and hydrophobic interactions. These interactions are enhanced by depletion interactions along the C-terminus, forming a tunable network of bonds that allow $A_{2A}R$ oligomers to adopt multiple interfaces. This study uncovers the disordered C-terminus as a prominent driving factor for the oligomerization of a GPCR, offering important guidance for structure-function studies of $A_{2A}R$ and other GPCRs.

INTRODUCTION

G protein-coupled receptors (GPCRs) have long been studied as monomeric units, but accumulating evidence demonstrates that these receptors can also form homo- and hetero-oligomers with far-reaching functional implications. The properties emerging from these oligomers can be distinct from those of the monomeric protomers in ligand binding(1–4), G protein

coupling(5–9), downstream signaling(10–13), and receptor internalization/desensitization(14–16). With the vast number of genes identified in the human genome(17), GPCRs are able to form a daunting number of combinations with unprecedented functional consequences. The existence of this intricate network of interactions among GPCRs presents major challenges and opportunities for the development of novel therapeutic approaches(18–23). Hence, it is crucial to identify the driving factors that govern the oligomerization of GPCRs, such that the properties of GPCR oligomers can be understood.

GPCR oligomers with multiple interfaces(24–28) can give rise to myriad ways by which these complexes can be formed and their functions modulated. In the crystal structure of the turkey β_1-adrenergic receptor (β_1AR), the receptor appears to dimerize via two different interfaces, one formed via TM4/TM5 (transmembrane domains 4/5) and the other via TM1/TM2/H8 (helix 8) contacts(29). Similarly, in the crystal structure of the antagonist-bound μ-opioid receptor (μ-OR), the protomers also dimerize via two interfaces; however, only one of them is predicted to induce a steric hindrance that prevents activation of both protomers(30), hinting at interface-specific functional consequences. A recent computational study predicted that the adenosine A_{2A} receptor (A_{2A}R) forms homodimers via three different interfaces and that the resulting dimeric architectures can modulate receptor function in different or even opposite ways(27). All of the above-mentioned interfaces are symmetric, meaning that the two protomers are in face-to-face orientations, hence forming strictly dimers. Asymmetric interfaces, reported in M_3 muscarinic receptor(31), rhodopsin(32–34), and opsin(34), are in contrast formed with the protomers positioning face-to-back, possibly enabling the association of higher-order oligomers.

Not only do GPCRs adopt multiple oligomeric interfaces, but various studies also suggest that these interfaces may dynamically rearrange to activate receptor function(35). According to a recent computational study, A_{2A}R oligomers can adopt eight different interfaces that interconvert when the receptor is activated or when there are changes in the local membrane environment(24). Similarly, a recent study that combined experimental and computational data proposed that neurotensin receptor 1 (NTS_1R) dimer is formed by “rolling” interfaces that co-exist and interconvert when the receptor is activated(36). Clearly, meaningful functional studies of GPCRs require exploring their dynamic, heterogeneous oligomeric interfaces.

The variable nature of GPCR oligomeric interfaces suggests that protomers of GPCR oligomers may be connected by tunable interactions. In this study, we explore the role of an intrinsically disordered region (IDR) of a model GPCR that could engage in diverse non-covalent interactions, such as electrostatic interactions, hydrogen bonds, or hydrophobic interactions. These non-covalent interactions are readily tunable by external factors, such as pH, salts, and solutes, and further can be entropically stabilized by depletion interactions(37–39), leading to structure formation and assembly(40–47). In a system where large protein molecules and small solute particles typically coexist in solution, assembly of the protein molecules causes their excluded volumes to overlap and the solvent volume accessible to the solutes to increase, raising the entropy of the system. The type and concentration of solutes or ions can also remove water from the hydration shell around the proteins, further enhancing entropy-driven protein-protein association in what is known as the hydrophobic effect(48). This phenomenon is applied in the precipitation of proteins upon addition of so-called salting-out ions according to the Hofmeister series(49). The ability of IDRs to readily engage in these non-covalent interactions motivates our focus on the potential role of IDRs in driving GPCR oligomerization.

The cytosolic carboxy (C-)terminus of GPCRs is usually an IDR(50, 51). Varying in length among different GPCRs, the C-terminus is commonly removed in structural studies of GPCRs to enhance receptor stability and conformational homogeneity. A striking example is $A_{2A}R$, a model GPCR with a particularly long, 122-residue, C-terminus that is truncated in all published structural biology studies(24, 27, 52–59). However, evidence is accumulating that such truncations—shown to affect GPCR downstream signaling(60–62)—may abolish receptor oligomerization(63, 64). A study using immunofluorescence has demonstrated that C-terminally truncated $A_{2A}R$ does not show protein aggregation or clustering on the cell surface, a process readily observed in the wild-type form(65). Our recent study employing a tandem three-step chromatography approach uncovered the impact of a single residue substitution of a C-terminal cysteine, C394S, in reducing the receptor homo-oligomerization *in vitro*(63). In the context of heteromerization, mass spectrometry and pull-down experiments have demonstrated that $A_{2A}R$-D_2R dimerization occurs via direct electrostatic interactions between the C-terminus of $A_{2A}R$ and the third intracellular loop of D_2R(66). These results all suggest that the C-terminus may participate in $A_{2A}R$ oligomer

formation. However, no studies to date have directly and systematically investigated the role of the C-terminus, or any IDRs, in GPCR oligomerization.

This study focuses on the homooligomerization of the human adenosine $A_{2A}R$, a model GPCR, and seeks to address: (i) whether the C-terminus engages in $A_{2A}R$ oligomerization, and if so, (ii) whether the C-terminus forms multiple oligomeric interfaces. We use size-exclusion chromatography (SEC) to assess the oligomerization levels of $A_{2A}R$ variants with strategic C-terminal modifications: mutations of a cysteine residue C394 and a cluster of charged residues ^{355}ERR^{357}, as well as systematic truncations at eight different sites along its length. We complemented our experimental study with an independent molecular dynamics study of $A_{2A}R$ dimers of five C-terminally truncated $A_{2A}R$ variants designed to mirror the experimental constructs. We furthermore examined the oligomerization level of select C-terminally modified $A_{2A}R$ variants under conditions of ionic strength ranging from 0.15 to 0.95 M. To test whether the C-termini directly and independently promote $A_{2A}R$ oligomerization, we recombinantly expressed the entire $A_{2A}R$ C-terminal segment sans the transmembrane portion of the receptor and investigated its solubility and assembly properties with increasing ion concentration and temperature. This is the first study designed to uncover the role of the intrinsically disordered C-terminus on the oligomerization of a GPCR.

RESULTS

This study systematically investigates the role of the C-terminus on $A_{2A}R$ oligomerization and the nature of the interactions involved through strategic mutations and truncations at the C-terminus as well as modulation of the ionic strength of solvent. The experimental assessment of $A_{2A}R$ oligomerization relies on size-exclusion chromatography (SEC) analysis.

Size Exclusion Chromatography Quantifies $A_{2A}R$ Oligomerization

We performed SEC analysis on a mixture of ligand-active $A_{2A}R$ purified from a custom synthesized antagonist affinity column (**Fig. S1A**). Distinct oligomeric species were separated and eluted in the following order: high-molecular-weight (HMW) oligomer, dimer, and monomer (**Fig. 1** and **Fig. S1B**). The population of each oligomeric species was quantified as the integral of each Gaussian from a multiple-Gaussian curve fit of the SEC signal. The reported standard errors were calculated from the variance of the fit that do not correspond to experimental errors (see **Table S1** and **Fig. S2** for SEC data corresponding to all $A_{2A}R$ variants in this study). As this study sought to identify the factors that promote $A_{2A}R$ oligomerization, the populations with oligomeric interfaces (*i.e.*, dimer and HMW oligomer) were compared with those without such interfaces (*i.e.*, monomer). Hence, the populations of the HMW oligomer and dimer were expressed relative to the monomer population in arbitrary units as monomer-equivalent concentration ratios, henceforth referred to as population levels (**Fig. 1)**.

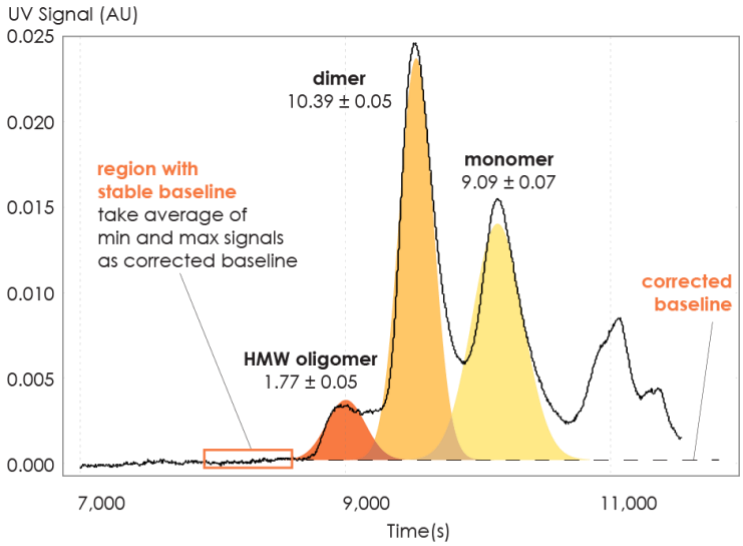

Figure 1. *Method for collecting SEC data and assessing $A_{2A}R$ oligomerization. The SEC data is recorded every second as absorbance at 280 nm. The baseline is corrected to ensure uniform fitting and integration across the peaks. The areas under the curve, resulting from a multiple-Gaussian curve fit, express the population of each oligomeric species. The reported standard errors of integration are within a 95% confidence interval and are calculated from the variance of the fit, not experimental errors. The levels of HMW oligomer and dimer are expressed relative to the monomeric population in arbitrary units. A representative calculation defining the oligomer levels is given in the box.*

C-Terminal Amino Acid Residue C394 Contributes to $A_{2A}R$ Oligomerization

To investigate whether the C-terminus of $A_{2A}R$ is involved in receptor oligomerization, we first examined the role of residue C394, as a previous study demonstrated that the mutation C394S dramatically reduced $A_{2A}R$ oligomer levels(63). The C394S mutation was replicated in our experiments, alongside other amino acid substitutions, namely alanine, leucine, methionine or valine, generating five $A_{2A}R$-C394X variants. The HMW oligomer and dimer levels of $A_{2A}R$ wild-type (WT) were compared with those of the $A_{2A}R$-C394X variants. We found that the dimer level of $A_{2A}R$-WT was significantly higher than that of the $A_{2A}R$-C394X variants (WT: 1.14; C394X: 0.24–0.57; **Fig. 2A**). A similar result, though less pronounced, was observed when the HMW oligomer and dimer levels were considered together (WT: 1.34; C394X: 0.59–1.21; **Fig. 2A**). This suggests that residue C394 plays a role in $A_{2A}R$ oligomerization and more so in $A_{2A}R$ dimers.

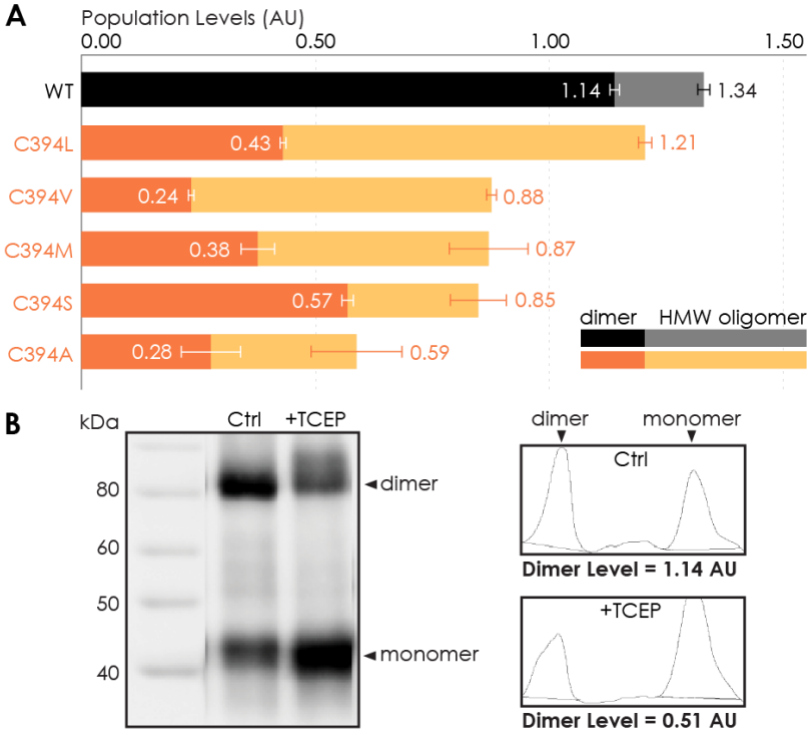

Figure 2. *Residue C394 helps stabilize $A_{2A}R$ oligomerization via disulfide bonds. (A) The effect of C394X substitutions on $A_{2A}R$ oligomerization. The levels of dimer (dark colors) and HMW oligomer (light colors) are expressed relative to the monomeric population in arbitrary units, with reported errors calculated from the variance of the fit, not experimental variation. (B) Line densitometry of Western Blot bands on SEC-separated dimeric population with and*

without 5 mM TCEP. The level of dimer is expressed relative to the monomeric population in arbitrary units similarly to the SEC analysis. MagicMark protein ladder (LC5602) is used as the molecular weight standard.

To test whether residue C394 stabilizes $A_{2A}R$ dimerization by forming disulfide linkages, we incubated SEC-separated $A_{2A}R$ dimer with 5 mM of the reducing agent TCEP, followed by SDS-PAGE and Western Blotting. The population of each species was determined as the area under the densitometric trace. The dimer level was then expressed as monomer-equivalent concentration ratios in a manner similar to that of the SEC experiment described above. Upon incubation with TCEP, the dimer level of the sample decreased from 1.14 to 0.51 (**Fig. 2B**). This indicates that disulfide bond formation via residue C394 is one possible mechanism for $A_{2A}R$ dimerization. However, a significant population of $A_{2A}R$ dimer remained resistant to TCEP and C394X mutations (**Fig. 2**), suggesting that disulfide linkages are not the only driving factor of $A_{2A}R$ oligomer formation. This finding agrees with a previous study showing that residue C394 in $A_{2A}R$ dimer is still available for nitroxide spin labeling,(63) suggesting that additional interfacial sites help drive $A_{2A}R$ dimer/oligomerization.

C-Terminus Truncation Systematically Reduces $A_{2A}R$ Oligomerization

To determine which interfacial sites in the C-terminus other than C394 drive $A_{2A}R$ dimer/oligomerization, we carried out systematic truncations at eight sites along the C-terminus (A316, V334, G344, G349, P354, N359, Q372, and P395), generating eight $A_{2A}R$-ΔC variants (**Fig. 3A**). The $A_{2A}R$-A316ΔC variant corresponds to the removal of the entire disordered C-terminal region as previously performed in all published structural studies(24, 27, 52–59). Using the SEC analysis described earlier (**Fig. 1**) we evaluated the HMW oligomer and dimer levels of the $A_{2A}R$-ΔC variants relative to that of the $A_{2A}R$ full-length-wild-type (FL-WT) control. Both the dimer and the total oligomer levels of $A_{2A}R$ decreased progressively with the shortening of the C-terminus, with almost no oligomerization detected upon complete truncation of the C-terminus at site A316 (**Fig. 3B**). This result shows that the C-terminus drives $A_{2A}R$ oligomerization, with multiple potential interaction sites positioned along much of its length.

Interestingly, there occurred a dramatic decrease in the dimer level between the N359 and P354 truncation sites, from a value of 0.81 to 0.19, respectively (**Fig. 3B**). A similar result, though less pronounced, was observed on the total oligomer level, with a decrease from 1.09 to 0.62 for the

N359 and P354 truncation sites, respectively (**Fig. 3B**). Clearly, the C-terminal segment encompassing residues 354–359 (highlighted in black in **Fig. 3A**) is a key constituent of the $A_{2A}R$ oligomeric interface.

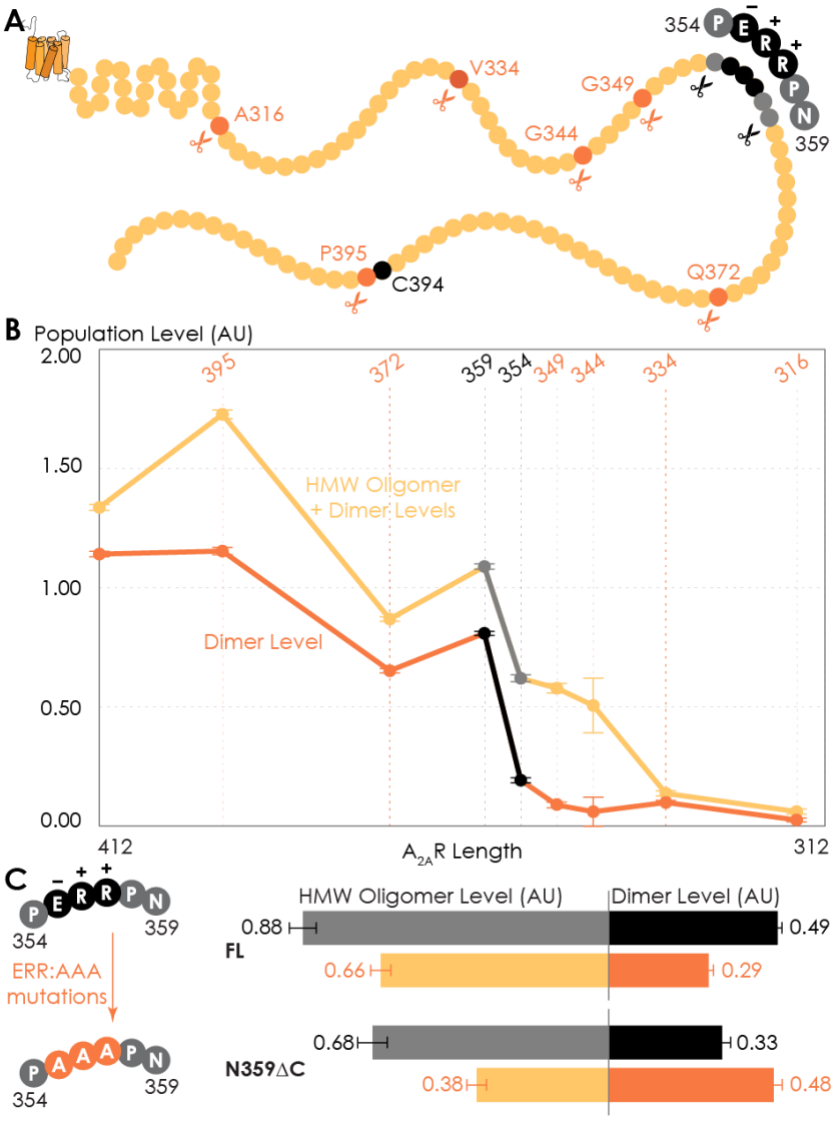

Figure 3. *Truncating the C-terminus systematically affects $A_{2A}R$ oligomerization. (A) Depiction of where the truncation points are located on the C-terminus, with region 354–359 highlighted (in black) showing critical residues. (B) The levels of dimer and HMW oligomer are expressed relative to the monomeric population as an arbitrary unit and plotted against the residue number of the truncation sites, with reported errors calculated from the variance of the fit, not experimental variation. Region 354–359 is emphasized (in black and gray) due to a drastic change in the dimer and HMW oligomer levels. (C) The dependence of $A_{2A}R$ oligomerization on three consecutive charged residues $^{355}ERR^{357}$. The substitution of residues $^{355}ERR^{357}$ to $^{355}AAA^{357}$ is referred to as the ERR:AAA mutations. The levels of*

dimer and HMW oligomer are expressed relative to the monomeric population as an arbitrary unit, with reported errors calculated from the variance of the fit, not experimental variation.

Since segment 354–359 contains three consecutive charged residues (^{355}ERR^{357}; **Fig. 3A**), which could be involved in electrostatic interactions, we hypothesized that this ^{355}ERR^{357} cluster could strengthen inter-protomer A_{2A}R-A_{2A}R association. To test this hypothesis, residues ^{355}ERR^{357} were substituted by ^{355}AAA^{357} on A_{2A}R-FL-WT and A_{2A}R-N359ΔC to generate A_{2A}R-ERR:AAA variants (**Fig. 3C**). We then compared the HMW oligomer and dimer levels of the resulting variants with controls (same A_{2A}R variants but without the ERR:AAA mutations). We found that the ERR:AAA mutations had varied effects on the dimer level: decreasing for A_{2A}R-FL-WT (ctrl: 0.49; ERR:AAA: 0.29) but increasing for A_{2A}R-N359ΔC (ctrl: 0.33; ERR:AAA: 0.48) (**Fig. 3C**). In contrast, the ERR:AAA mutations reduced the HMW oligomer level of both A_{2A}R-FL-WT (ctrl: 0.88; ERR:AAA: 0.66) and A_{2A}R-N359ΔC (ctrl: 0.68; ERR:AAA: 0.38) (**Fig. 3C**). Consistently, the ERR:AAA mutation lowered the total oligomer level of both A_{2A}R-FL-WT (ctrl: 1.37; ERR:AAA: 0.94) and A_{2A}R-N359ΔC (ctrl: 1.01; ERR:AAA: 0.85) (**Fig. 3C**). These results suggest that the charged residues ^{355}ERR^{357} participate in A_{2A}R oligomerization, with a greater effect in the context of a longer C-terminus and for higher-order oligomer formation. The question then arises as to what types of interactions are formed along the C-terminus that help stabilize A_{2A}R oligomerization.

C-Terminus Truncation Disrupts Complex Network of Non-Bonded Interactions Necessary for A_{2A}R Dimerization.

Given that the structure of A_{2A}R dimers or oligomers are unknown, we next used molecular dynamics (MD) simulations to seek molecular-level insights into the role of the C-terminus in driving A_{2A}R dimerization and to determine the specific interaction types and sites involved in this process. First, to explore A_{2A}R dimeric interface, we performed coarse-grained (CG) MD simulations, which can access the length and time scales relevant to membrane protein oligomerization, albeit at the expense of atomic-level details. We carried out a series of CGMD simulations on five A_{2A}R-ΔC variants designed to mirror the experiments by systematic truncation at five sites along the C-terminus (A316, V334, P354, N359, and C394). Our results revealed that A_{2A}R dimers were formed with multiple interfaces, all involving the C-terminus (**Fig. 4A** and **S3A**).

The vast majority of $A_{2A}R$ dimers were symmetric, with the C-termini of the protomers directly interacting with each other. A smaller fraction of the dimers had asymmetric orientations, with the C-terminus of one protomer interacting with other parts of the other protomer, such as ICL2 (the second intracellular loop), ICL3, and ECL2 (the second extracellular loop) (**Fig. 4A**).

Our observation of multiple $A_{2A}R$ oligomeric interfaces, consistent with previous studies(24, 27), suggests that tunable, non-covalent intermolecular interactions are involved in receptor dimerization. We dissected two key non-covalent interaction types: electrostatic and hydrogen bonding interactions. (The criteria for designating inter-$A_{2A}R$ contacts as electrostatic interactions or hydrogen bonds are described in detail in **Materials and Methods.**) Electrostatic interactions were calculated from CGMD simulations. Hydrogen bonds were quantified from atomistic MD simulation, given that the CG model merges all hydrogens into a coarse-grained bead and hence cannot report on hydrogen bonds. This analysis was performed on the symmetric dimers as they constituted the majority of the assemblies. With the least truncated $A_{2A}R$ variant containing the longest C-terminus, $A_{2A}R$-C394ΔC, we observed an average of 15.9 electrostatic contacts (**Fig. 4B**) and 26.7 hydrogen bonds (**Fig. 4C**) between the C-termini of the protomers. This result shows that both electrostatic interactions and hydrogen bonds play important roles in $A_{2A}R$ dimer formation.

Upon further C-terminus truncation, the average number of both electrostatic contacts and hydrogen bonds involving C-terminal residues progressively declined, respectively reaching 5.4 and 6.0 for $A_{2A}R$-A316ΔC (in which the disordered region of the C-terminus is removed) (**Fig. 4B** and **4C**). This result is consistent with the experimental result, which demonstrated a progressive decrease of $A_{2A}R$ oligomerization with the shortening of the C-terminus (**Fig. 3B**). Interestingly, upon systematic truncation of the C-terminal segment 335–394, we observed in segment 291–334 a steady decrease in the average number of electrostatic contacts, from 10.4 to 7.4 (**Fig. 4B**). This trend was even more pronounced with hydrogen bonding contacts involving segment 291–334 decreasing drastically from 21.0 to 7.0 as segment 335–394 was gradually removed (**Fig. 4C**). This observation, namely that truncation of a C-terminal segment reduces inter-$A_{2A}R$ contacts elsewhere along the C-terminus, indicates that a cooperative mechanism of dimerization exists, in which an extended C-terminus of $A_{2A}R$ stabilizes inter-$A_{2A}R$ interactions near the heptahelical bundles of the dimeric complex. Besides the intermolecular interactions, we also identified a

network of intramolecular salt bridges involving residues on the C-termini, including cluster ^{355}ERR^{357} (**Fig. 7A**). These results demonstrate that $A_{2A}R$ dimers can be formed via multiple interfaces predominantly in symmetric orientations, facilitated a cooperative network of electrostatic interactions and hydrogen bonds along much of its C-terminus.

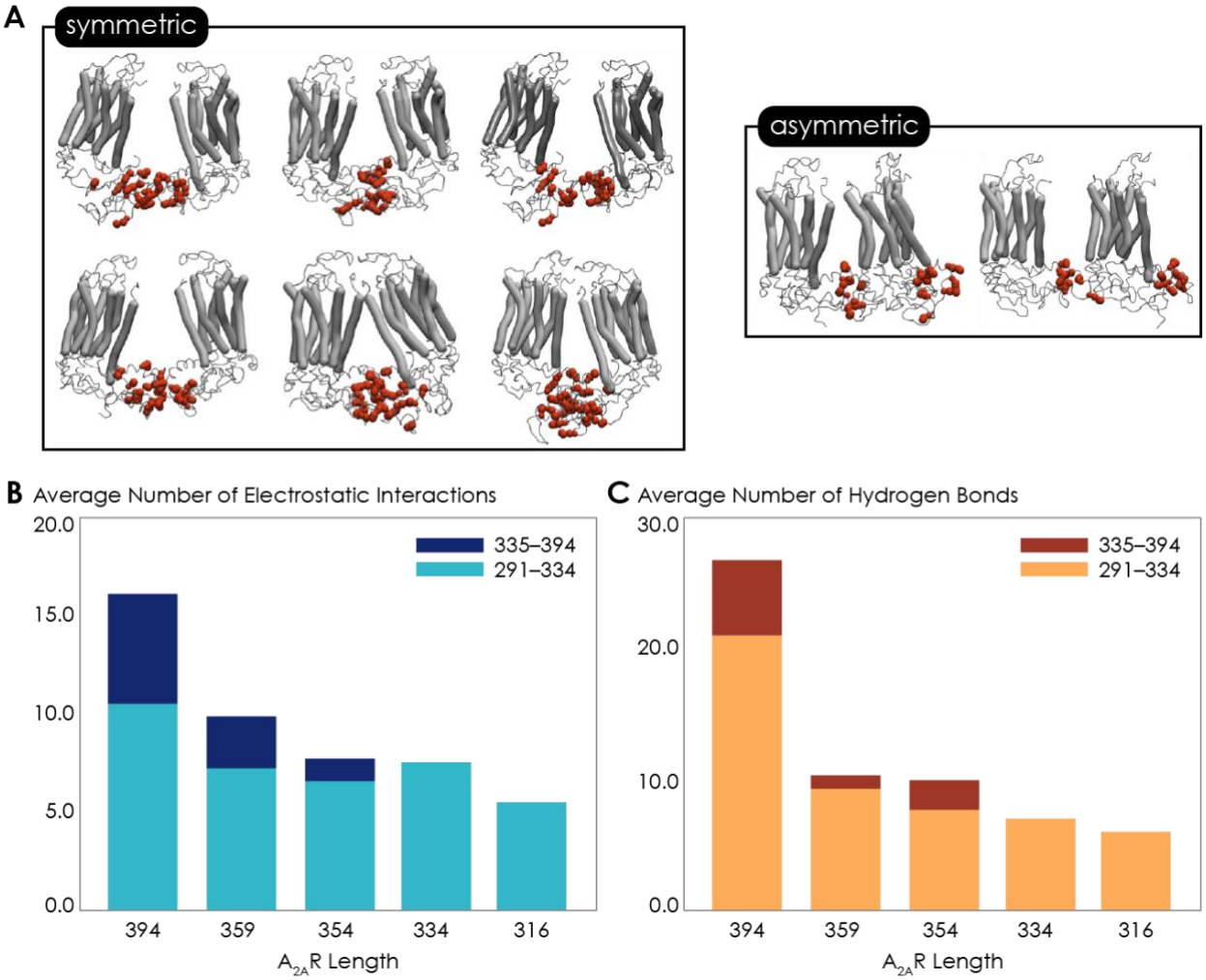

Figure 4. *Non-bonded interactions of the extended C-terminus of $A_{2A}R$ play a critical role in stabilization of the dimeric interface.* ***(A)*** *Dimer configurations from cluster analysis in GROMACS of the 394-residue variant identify two major clusters involving either 1) the C-terminus of one protomer and the C-terminus, ICL2, and ICL3 of the second protomer or 2) the C-terminus of one protomer and ICL2, ICL3, and ECL2 of the second protomer. Spheres: residues forming intermolecular electrostatic contacts.* ***(B)*** *Average number of residues that form electrostatic contacts as a function of sequence length of $A_{2A}R$.* ***(C)*** *Average number of residues that form hydrogen bonds as a function of sequence length of $A_{2A}R$.*

Ionic Strength Modulates Oligomerization of C-Terminally Truncated $A_{2A}R$ Variants

So far, we have demonstrated that the C-terminus clearly plays a role in forming $A_{2A}R$ oligomeric interfaces. However, the driving factors of $A_{2A}R$ oligomerization remain unknown. The variable nature of $A_{2A}R$ oligomeric interfaces suggests that the main driving forces must be non-covalent interactions, such as electrostatic interactions and hydrogen bonds as identified by the above MD simulations. Modulating the solvent ionic strength is an effective method to identify the types of non-covalent interaction(s) at play. Specifically, with increasing ionic strength, electrostatic interactions can be weakened (based on Debye-Hückel theory, most electrostatic bonds at a distance greater than 5 Å are screened out at an ionic strength of 0.34 M at 4°C), depletion interactions are enhanced with salting-out salts, and hydrogen bonds remain relatively impervious. For this reason, we subjected various $A_{2A}R$ variants (FL-WT, FL-ERR:AAA, N359ΔC, and V334ΔC) to ionic strength ranging from 0.15 to 0.95 M by adding NaCl (buffer composition shown in **Table 1)**. The HMW oligomer and dimer levels of the four $A_{2A}R$ variants were determined and plotted as a function of ionic strengths.

The low ionic strength of 0.15 M should not affect hydrogen bonds or electrostatic interactions, if present. We found that the dimer and total oligomer levels of all four variants were near zero (**Fig. 5**). This is a striking observation, as it already excludes electrostatic and hydrogen-bonding interactions as the dominant force for $A_{2A}R$ association. The question remains whether depletion interactions could be involved.

At higher ionic strengths of 0.45 M and 0.95 M, the dimer and total oligomer levels of $A_{2A}R$-V334ΔC still remained near zero (**Fig. 5)**. In contrast, we observed a progressive and significant increase in the dimer and total oligomer levels of $A_{2A}R$-FL-WT with increasing ionic strength (**Fig. 5)**. This result indicates $A_{2A}R$ oligomerization must be driven by depletion interactions, which are enhanced with increasing ionic strength, and that these interactions involve the C-terminal segment after residue V334.

Upon closer examination, we recognize that at the very high ionic strength of 0.95 M, the increase in the dimer and total oligomer levels was robust for $A_{2A}R$-FL-WT, but less pronounced for $A_{2A}R$-FL-ERR:AAA (**Fig. 5**). Furthermore, this high ionic strength even had an opposite effect on $A_{2A}R$-N359ΔC, with both its dimer and total oligomer levels abolished (**Fig. 5**). These results indicate

that the charged cluster ^{355}ERR^{357} and the C-terminal segment after residue N359 are required for depletion interactions to promote $A_{2A}R$ oligomerization to the full extent.

Taken together, we demonstrated that $A_{2A}R$ oligomerization is more robust when the C-terminus is fully present and the ionic strength is higher, suggesting that depletion interactions via the C-terminus are a strong driving factor of $A_{2A}R$ oligomerization. The question then arises whether such depletion interactions are the result of the C-termini directly interacting with one another, necessitating an experiment that investigates the behavior of $A_{2A}R$ C-terminus sans the transmembrane domains.

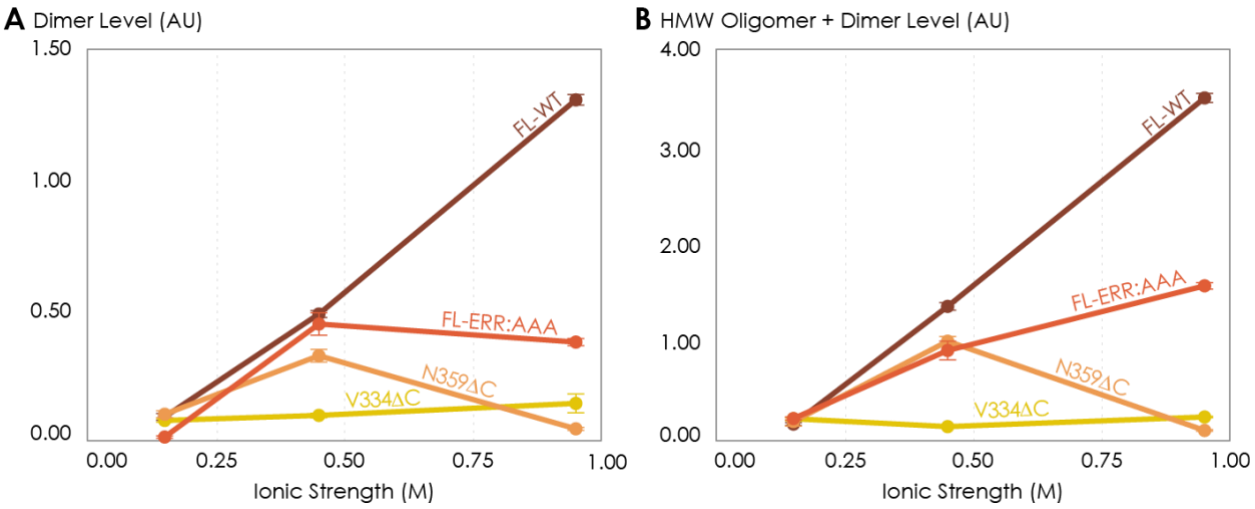

Figure 5. *The effects of ionic strength on the oligomerization of various $A_{2A}R$ variants reveal the involvement of depletion interactions. The levels of dimer and HMW oligomer are expressed relative to the monomeric population as an arbitrary unit and plotted against ionic strength, with reported errors calculated from the variance of the fit, not experimental variation. NaCl concentration is varied to achieve ionic strengths of 0.15, 0.45, and 0.95 M.*

The Isolated $A_{2A}R$ C-Terminus Is Prone to Aggregation

To test whether $A_{2A}R$ oligomerization is driven by direct depletion interactions among the C-termini of the protomers, we assayed the solubility and assembly properties of the stand-alone $A_{2A}R$ C-terminus—an intrinsically disordered peptide—sans the upstream transmembrane regions. Since depletion interactions can be manifested via the hydrophobic effect(48), we examined whether this effect can cause $A_{2A}R$ C-terminal peptides to associate.

It is an active debate(67) whether the hydrophobic effect can be promoted or suppressed by ions with salting-out or salting-in tendency, respectively(68–70). We increased the solvent ionic strength using either sodium (salting-out) or guanidinium (salting-in) ions and assessed the aggregation propensity of the C-terminal peptides using UV-Vis absorption at 450 nm. We first observed the behavior of the C-terminus with increasing salting-out NaCl concentrations. At NaCl concentrations below 1 M, the peptide was dominantly monomeric, despite showing slight aggregation at NaCl concentrations between 250–500 mM (**Fig. 6A**). At NaCl concentrations above 1 M, $A_{2A}R$ C-terminal peptides strongly associated into insoluble aggregates (**Fig. 6A**). Consistent with the observations made with the intact receptor (**Fig. 5**), $A_{2A}R$ C-terminus showed the tendency to progressively precipitate with increasing ionic strengths, suggesting that depletion interactions drive the association and precipitation of the peptides. We next observed the behavior of the C-terminus with increasing concentrations of guanidine hydrochloride (GdnHCl), which contains salting-in cations that do not cause proteins to precipitate and instead facilitate the solubilization of proteins(71, 72). Our results demonstrated that the $A_{2A}R$ C-terminus incubated in 4 M GdnHCl showed no aggregation propensity (**Fig. 6A)**, validating our expectation that depletion interactions are not enhanced by salting-out salts. These observations demonstrate that the C-terminal peptide in and of itself can directly interact with other C-terminal peptides to form self-aggregates in the presence of ions, and presumably solutes, that have salting-out effects.

Attractive hydrophobic interactions among the hydrophobic residues are further enhanced by water solvating the protein having more favorable interactions with other water molecules, ions or solutes than with the protein, here the truncated C-terminus(73–75). We explored the possible contribution of hydrophobic interactions to the aggregation of the C-terminal peptides using differential scanning fluorimetry (DSF). In particular, we gradually increased the temperature to melt the C-terminal peptides, exposing any previously buried hydrophobic residues (**Fig. S4A**) which then bound to the SYPRO orange fluorophore, resulting in an increase in fluorescence signal. Our results showed that as the temperature increased, a steady rise in fluorescence was observed (**Fig. 6B**), indicating that multiple hydrophobic residues were gradually exposed to the SYPRO dye. However, at approximately 65°C, the melt peak signal was abruptly quenched (**Fig. 6B**), indicating that the hydrophobic residues were no longer exposed to the dye. This observation suggests that, at 65°C, enough hydrophobic residues in the C-terminal peptides were exposed such

that they collapsed on one another (thus expelling the bound dye molecules), resulting in aggregation. Clearly, the hydrophobic effect can cause $A_{2A}R$ C-terminal peptides to directly associate. These results demonstrate that $A_{2A}R$ oligomer formation can be driven by depletion interactions among the C-termini of the protomers.

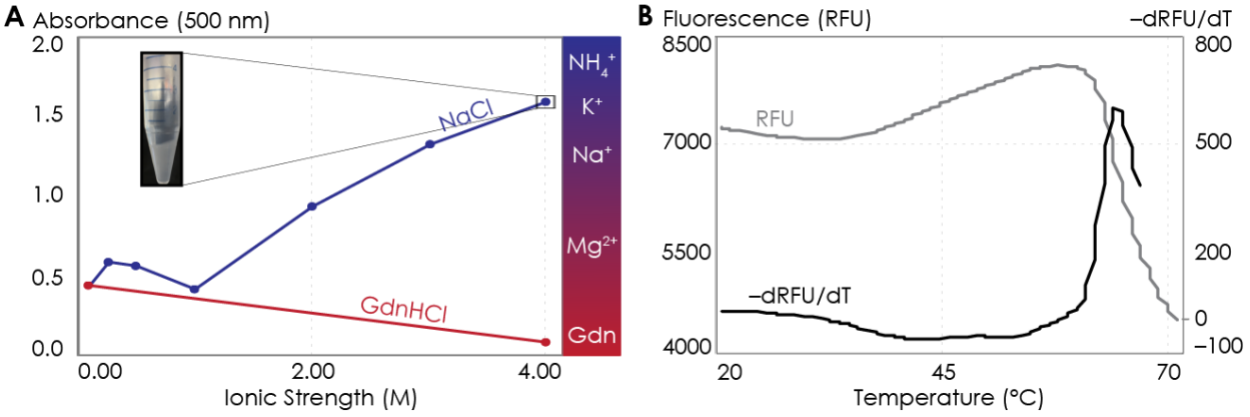

Figure 6. *The $A_{2A}R$ C-terminus is prone to aggregation. (A) Absorbance at 500 nm of the $A_{2A}R$ C-terminus in solution, with NaCl and GdnHCl concentrations varied to achieve ionic strengths 0–4 M. Inset: the solution at ionic strength 4 M achieved with NaCl. The Hofmeister series is provided to show the ability of cations to salt out (blue) or salt in (red) proteins. (B) SYPRO orange fluorescence of solutions containing the $A_{2A}R$ C-terminus as the temperature was varied from 20 to 70°C (grey). The change in fluorescence, measured in relative fluorescence unit (RFU), was calculated by taking the first derivative of the fluorescence curve (black).*

DISCUSSION

The key finding of this study is that the C-terminus of $A_{2A}R$, removed in all previously published structural studies of this receptor, is directly responsible for receptor oligomerization. Using a combination of experimental and computational approaches, we demonstrate that the C-terminus drives $A_{2A}R$ oligomerization via a combination of disulfide linkages, hydrogen bonds, electrostatic interactions, and hydrophobic interactions. This diverse combination of interactions is greatly enhanced by depletion interactions, forming a network of malleable bonds that give rise to the existence of multiple $A_{2A}R$ oligomeric interfaces.

The intermolecular disulfide linkages associated with residue C394 play a role in $A_{2A}R$ oligomerization. However, it is unclear which cysteine on the second protomer is linked to this cysteine. A previous study showed that residue C394 in $A_{2A}R$ dimer is available for nitroxide spin

labeling(63), suggesting that some of these disulfide bonds may be between residue C394 and another cysteine in the hydrophobic core of $A_{2A}R$ that do not form intramolecular disulfide bonds(76–78). Many examples exist where disulfide linkages help drive GPCR oligomerization, including the CaR-$mGluR_1$ heterodimer(79), homodimers of $mGluR_5$(80), M_3R(81), V_2R(82), 5-HT_4R(83) and 5-$HT_{1D}R$(84), and even higher-order oligomers of D_2R(85). However, although unconventional cytoplasmic disulfide bonds have been reported(86, 87), no study has shown how such linkages would be formed *in vivo*, as the cytoplasm lacks the conditions and machinery required for disulfide bond formation(88–91). Nevertheless, residue C394 is highly conserved and a C-terminal cysteine is almost always present among $A_{2A}R$ homologs(92), suggesting that this cysteine cannot be excluded for serving an important role *in vivo*.

The electrostatic interactions that stabilize $A_{2A}R$ oligomer formation come from multiple sites along the C-terminus. From a representative snapshot of a $A_{2A}R$-C394ΔC dimer from our MD simulations (**Fig. 7A**), we could visualize not only the intermolecular interactions calculated from the CGMD simulations (**Fig. 4B**), but also intramolecular salt bridges. In particular, the ^{355}ERR^{357} cluster of charged residues lies distal from the dimeric interface, yet still forms several salt bridges (**Fig. 7A**, inset). This observation is supported by our experimental results showing that substituting this charged cluster with alanines reduces the total $A_{2A}R$ oligomer levels (**Fig. 3C**). However, it is unclear how such salt bridges involving this ^{355}ERR^{357} cluster are enhanced by depletion interactions (**Fig. 5**), as electrostatic interactions are usually screened out at high ionic strengths. In our MD simulations, we also observed networks of salt bridges along the dimeric interface, for example between K315 of one monomer and D382 and E384 of the other monomer (**Fig. 7A**, inset). The innate flexibility of the C-terminus could facilitate the formation of such salt bridges, which then acts as a potential scaffold to stabilize $A_{2A}R$ dimers.

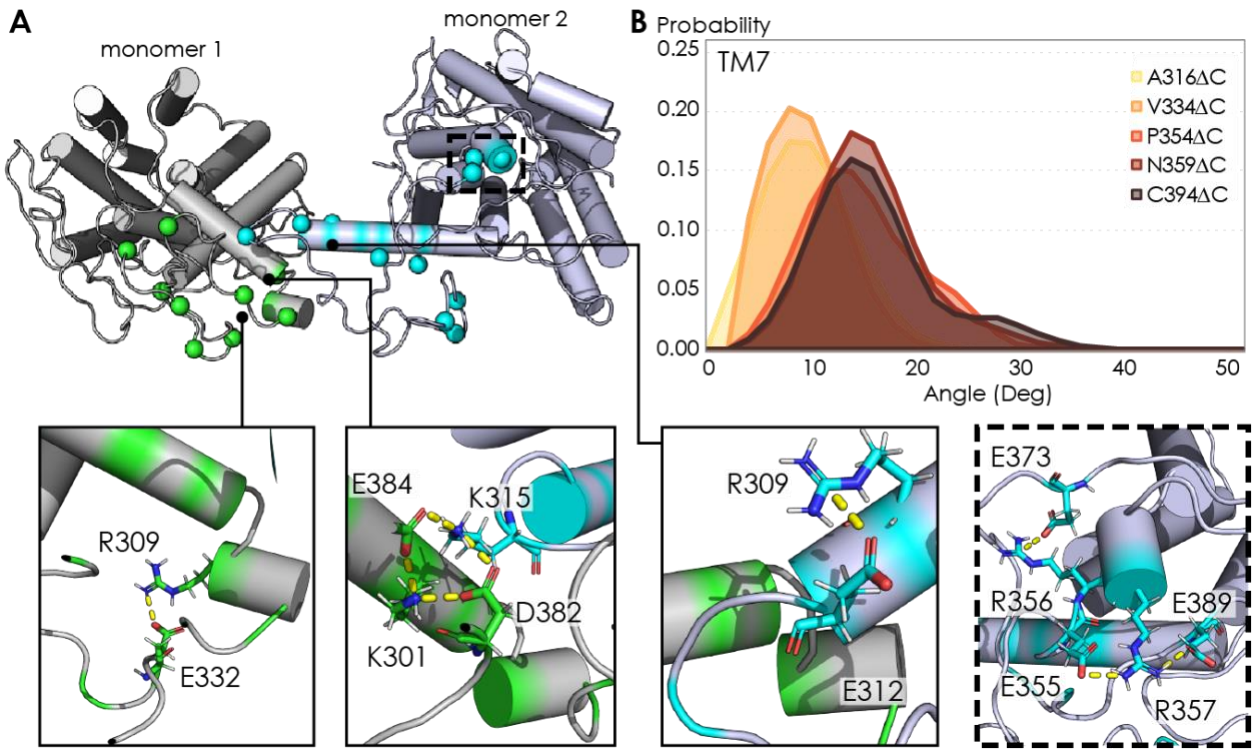

Figure 7. (A) *Representative snapshot of A_{2A}R-C394ΔC dimers shows salt bridge formation between a sample trajectory. The insets are close-ups of the salt bridges, which can be both intra- and intermolecular. The last inset shows a network of salt bridges with the charged cluster ^{355}ERR^{357} involved.* ***(B)*** *Helical tilt angles for TM7 helix in A_{2A}R as a function of protein length. Systematic truncations of the C-terminus lead to rearrangement of the heptahelical bundle. The participation of the C-terminus in A_{2A}R dimerization increases the tilting of the TM7 domain, which is in closest proximity to the C-terminus.*

We also found that depletion interactions can enhance the diversity of interactions that stabilize A_{2A}R oligomer formation (**Fig. 5** and **6**). Depletion interactions could be the key factor to the cooperative mechanism by which A_{2A}R oligomerization occurs. As revealed by our MD simulations, an increasing number of contacts are formed along segment 291–334 when the rest of C-terminus is present (**Fig. 4B** and **4C)**. As more of the C-terminus is preserved, the greater extent of depletion interactions limits the available dimer arrangements, forcing segment 291–334 into an orientation that optimizes intermolecular interactions.

Our finding that A_{2A}R forms homo-oligomers via multiple interfaces (**Fig. 4A**) agrees with the increasing number of studies reporting multiple and interconverting oligomeric interfaces in A_{2A}R and other GPCRs(24–36). When translated to *in vivo* situations, GPCR oligomers can also

transiently associate and dissociate(93–96). Such fast conformational changes require that the oligomeric interfaces be formed by interactions that can easily be modulated. This is consistent with our study, which demonstrates that depletion interactions via the intrinsically disordered, malleable C-terminus drive $A_{2A}R$ oligomerization. Because depletion interactions can be readily tuned by environmental factors, such as ionic strength, molecular crowding, and temperature, the formation of GPCR oligomeric complexes could be dynamically modulated in response to environmental cues to regulate receptor function.

Not only did we find multiple $A_{2A}R$ oligomeric interfaces, we also found that these interfaces can be either symmetric or asymmetric. This finding is supported by a growing body of evidence that there exists both symmetric and asymmetric oligomeric interfaces for $A_{2A}R$(24) and many other GPCRs. Studies using various biochemical and biophysical techniques have shown that heterotetrameric GPCR complexes can be formed by dimers of dimers, including μOR-δOR(97), CXC_4R-CC_2R(98), CB_1R/D_2R(99) as well as those involving $A_{2A}R$, such as A_1R-$A_{2A}R$(61, 100) and $A_{2A}R$-D_2R(101). The quaternary structures identified in these studies required specific orientations of each protomer, with the most viable model involving a stagger of homodimers with symmetric interfaces(102). On the other hand, since symmetric interfaces limit the degree of receptor association to dimers, the HMW oligomer of $A_{2A}R$ observed in this(24) and other studies(63, 103) can only be formed via asymmetric interfaces. It is indeed tempting to suggest that the formation of the HMW oligomer of $A_{2A}R$ may even arise from combinations of different interfaces. In any case, the wide variation of GPCR oligomerization requires the existence of both symmetric and asymmetric oligomeric interfaces.

In the case of $A_{2A}R$, displacement of the transmembrane domains have been demonstrated to be the hallmark of receptor activation(104–107). However, no studies have linked receptor oligomerization with the arrangement of the TM bundles in $A_{2A}R$. Our MD simulations revealed that C-terminus truncation resulted in structural changes in the heptahelical bundles of $A_{2A}R$ dimers. Specifically, as more of the C-terminus was preserved, we observed a progressive increase in the helical tilt of TM7 (**Fig. 7B**). This change in helical tilt occurred for the entire heptahelical bundle, with an increase in tilt for TM1, TM2, TM3, TM5, and TM7, and a decrease in tilt for TM4 and TM6 (**Fig. S3**). The longer C-terminus in the full-length $A_{2A}R$ permits greater rearrangements in the transmembrane regions, leading to the observed change in helical tilt. This

result hints at potential conformational changes of $A_{2A}R$ upon oligomerization, necessitating future investigation on functional consequences.

C-terminal truncations prior to crystallization and structural studies may be the main reason for the scarcity of GPCR structures featuring oligomers. In that context, this study offers valuable insights and approaches to tune the oligomerization of $A_{2A}R$ and potentially of other GPCRs using its intrinsically disordered C-terminus. The presence of $A_{2A}R$ oligomeric populations with partial C-terminal truncations means that one can now study its oligomerization with less perturbation from the C-terminus. We also present evidence that the multiple C-terminal interactions that drive $A_{2A}R$ oligomerization can be easily modulated by ionic strength and specific salts (**Fig. 5** and **6**). Given that ~75% and ~15% of all class-A GPCRs possess a C-terminus of > 50 and > 100 amino acid residues(108), respectively, it will be worthwhile to explore the prospect of tuning GPCR oligomerization not only by shortening the C-terminus but also with simpler approaches such as modulating ionic strength and the surrounding salt environment.

CONCLUSION

This study emphasizes for the first time the definite impact of the C-terminus on $A_{2A}R$ oligomerization, which can be extended to include the oligomers formed by other GPCRs with a protracted C-terminus. We have shown that the oligomerization of $A_{2A}R$ is strongly driven by depletion interactions along the C-terminus, further modulating and enhancing the multiple interfaces formed via a combination of hydrogen, electrostatic, hydrophobic, and covalent disulfide interactions. The task remains to link $A_{2A}R$ oligomerization to functional roles of the receptor(109). From a structural biology standpoint, visualizing the multiple oligomeric interfaces of $A_{2A}R$ in the presence of the full-length C-terminus is key to investigating whether these interfaces give rise to different oligomer functions.

MATERIALS AND METHODS

Cloning, Gene Expression, and Protein Purification

The multi-integrating pITy plasmid(110), previously used for overexpression of $A_{2A}R$ in *Saccharomyces cerevisiae*(111), was employed in this study. pITy contains a Gal1–10 promoter

for galactose-induced expression, a synthetic pre-pro leader sequence which directs protein trafficking(112, 113), and the yeast alpha terminator. The genes encoding $A_{2A}R$ variants with 10-His C-terminal tag were cloned into pITy downstream of the pre-pro leader sequence, using either splice overlapping extension(114) or USER cloning using X7 polymerase(115, 116), with primers provided in **Table S3**. The plasmids were then transformed into *S. cerevisiae* strain BJ5464 (MATα ura3-52 trp1 leu2Δ1 his3Δ200 pep4::HIS3 prb1Δ1.6R can1 GAL) (provided by the lab of Anne Robinson at Carnegie Mellon University) using the lithium-acetate/PEG method(117). Transformants were selected on YPD G-418 plates (1% yeast extract, 2% peptone, 2% dextrose, 2.0 mg/mL G-418).

Receptor was expressed and purified following the previously described protocol(118). In brief, from freshly streaked YPD plates (1% yeast extract, 2% peptone, 2% dextrose), single colonies were grown in 5-mL YPD cultures over night at 30ºC. From these 5-mL cultures, 50-mL cultures were grown with a starting OD of 0.5 over night at 30ºC. To induce expression, yeast cells from these 50-mL cultures were centrifuged at 3,000 *x g* to remove YPD before resuspended in YPG medium (1% yeast, 2% peptone, 2% D-galactose) at a starting OD of 0.5. The receptor was expressed for 24 hours over night at 30ºC with 250 r.p.m shaking. Cells were pelleted by centrifugation at 3,000 *x g*, washed in sterile PBS buffer, and pelleted again before storage at –80ºC until purification.

Mechanical bead lysis of cells was done, per 250 mL of cell culture, by performing 12 pulses of 60 s intense vortexing (with at least 60 s of rest in between pulses) in 10 mL 0.5-mm zirconia silica beads (BioSpec, Bartlesville, OK, USA; #11079105z), 25 mL of lysis buffer (50 mM sodium phosphate, 300 mM sodium chloride, 10% (v/v) glycerol, pH = 8.0, 2% (w/v) n-Dodecyl-β-D-maltopyranoside (DDM; Anatrace, Maumee, OH, USA; #D310), 1% (w/v) 3-[(3-Cholamidopropyl)dimethylammonio]-1-propanesulfonate (CHAPS; Anatrace; #C216), and 0.2% (w/v) cholesteryl hemisuccinate (CHS; Anatrace; #CH210) and an appropriate amount of 100x Pierce Halt EDTA-free protease inhibitor (Pierce, Rockford, IL, USA #78439)). Beads were separated using a Kontex column. Unlysed cells were removed by centrifugation at 3,220 *x g* for 10 min. Receptor was let solubilized on rotary mixer for 3 hours before cell debris was removed by centrifugation at 10,000 *x g* for 30 min. Solubilized protein was incubated with Ni-NTA resin (Pierce; #88221) over night. Protein-resin mixture was then washed extensively in purification

buffer (50 mM sodium phosphate, 300 mM sodium chloride, 10% (v/v) glycerol, 0.1% (w/v) DDM, 0.1% (w/v) CHAPS and 0.2% (w/v) CHS, pH = 8.0) containing low imidazole concentrations (20–50 mM). $A_{2A}R$ was eluted into purification buffer containing 500 mM imidazole. Prior to further chromatographic purification, imidazole was removed using a PD-10 desalting column (GE Healthcare, Pittsburgh, PA, USA; # 17085101).

Ligand affinity resin was prepared as previously described for purification of active $A_{2A}R$.(119), (120) In brief, 8 mL of isopropanol-washed Affigel 10 resin (BioRad; # 1536099) was mixed gently in an Erlenmeyer flask for 20 h at room temperature with 48 mL of DMSO containing 24 mg of xanthine amine congener (XAC, high-affinity $A_{2A}R$ antagonist, K_D = 32 nM; Sigma, St. Louis, MO, USA; #X103). The absorbance at 310 nm of the XAC-DMSO solution before and after the coupling reaction was measured in 10 mM HCl and compared to a standard curve. The amount of resin bound to ligand was estimated to be 5.6 μM. The coupling reaction was quenched by washing the resin with DMSO, then with Tris-HCl 50 mM (pH = 7.4), then with 20% (v/v) ethanol. The resin was packed into a Tricorn 10/50 column (GE Healthcare) under pressure via a BioRad Duoflow FPLC (BioRad).

For purification of active $A_{2A}R$, the column was equilibrated with 4 CV of purification buffer. The IMAC-purified $A_{2A}R$ was desalted and diluted to 5.5 mL before applied to a 5-mL sample loop on the BioRad Duoflow FPLC, from which the sample was loaded onto the column at a rate of 0.1 mL/min. Inactive $A_{2A}R$ was washed from the column by flowing 10 mL of purification buffer at 0.2 mL/min, followed by 16 mL at 0.4 mL/min. Active $A_{2A}R$ was eluted from the column by flowing purification buffer containing 20 mM theophylline (low-affinity $A_{2A}R$ antagonist, K_D = 1.6 μM; Sigma, St. Louis, MO, USA; #T1633). Western blot analysis was performed to determine 4-mL fractions with active $A_{2A}R$ collected with a BioFrac fraction collector (BioRad; Hercules, CA, USA), which were then concentrated through a 30-kDa MWCO centrifugal filter (Millipore, Billerica, MA, USA; # UFC803096) and desalted to remove excess theophylline. For the experiments where the salt concentrations were varied, the buffer exchange was done also by this last desalting step.

Size-Exclusion Chromatography

To separate oligomeric species of active $A_{2A}R$, a prepacked Tricorn Superdex 200 10/300 GL column (GE Healthcare) connected to a BioRad Duoflow FPLC was equilibrated with 60 mL of running buffer (150 mM sodium chloride, 50 mM sodium phosphate, 10% (v/v) glycerol, 0.1% (w/v) DDM, 0.1% (w/v) CHAPS, 0.02% (w/v) CHS, pH = 8.0) at a flow rate of 0.2 mL/min. 0.5-mL fractions were collected with a BioFrac fraction collector in 30 mL of running buffer at the same flow rate. Analysis of SDS/PAGE and western blot was done to determine oligomeric states of the eluted $A_{2A}R$.

SEC Peak Analysis

SEC chromatograms were analyzed using OriginLab using the nonlinear curve fit (Gaussian) function. The area under the curve and the peak width were manually defined in cases where the SNR of the SEC trace were too low. The R^2 values reached > 0.96 for most cases. The population of each oligomeric species was expressed as the integral of each Gaussian this curve fit of the SEC signal. The HMW oligomer peak in some cases could not be fitted with one curve and thus was fitted with two curves instead. The reported standard errors were calculated from the variance of the fit and did not correspond to experimental errors. The results are detailed in **Fig. S2** and **Table S1**.

SDS-PAGE and Western Blotting

10% SDS-PAGE gels were hand-casted in BioRad Criterion empty cassettes (BioRad; #3459902, 3459903). Lysate controls were prepared by lysis of 5 OD cell pellets with 35 μL of YPER (Fisher Scientific, Waltham, MA, USA # 8990) at RT for 20 min, incubation with 2x Laemmli buffer (4% (w/v) SDS, 16% (v/v) glycerol, 0.02% (w/v) bromophenol blue, 167 M Tris, pH 6.8) at 37ºC for 1 h, and centrifugation at 3,000 *x g* for 1 min to pellet cell debris. Protein samples were prepared by incubation with 2x Laemmli buffer at 37ºC for 30 min. For all samples, 14 μL (for 26-well gel) or 20 μL (for 18-well gel) was loaded per lane, except for 7 μL of Magic Mark XP Western protein ladder (Thermo Scientific, Waltham, MA, USA; # LC5602) as a standard. Electrophoresis was carried out at 120 V for 100 min. Proteins were transferred to 0.2-μm nitrocellulose membranes (BioRad; # 170-4159) via electroblotting using a BioRad Transblot Turbo, mixed MW protocol. Membranes were blocked in Tris-buffered saline with Tween (TBST; 150 mM sodium chloride,

15.2 mM Tris-HCl, 4.6 mM Tris base, pH = 7.4, 0.1% (v/v) Tween 20 (BioRad; # 1706531)) containing 5% (w/v) dry milk, then probed with anti-$A_{2A}R$ antibody, clone 7F6-G5-A2 (Millipore, Burlington, MA, USA; # 05-717) at 1:500 in TBST with 0.5% (w/v) dry milk. Probing with secondary antibody was done with a fluorescent DyLight 550 antibody (Abcam, Cambridge, MA, USA; ab96880) at 1:600 in TBST containing 0.5% (w/v) milk.

Western blot was analyzed with Fiji. The Gels analysis plugin was used to define each sample lane, and to generate an intensity profile. Peaks were manually selected and integrated with the measure tool to determine the amount of protein present.

Coarse-Grained MD Simulations

Initial configuration of $A_{2A}R$ was based on the crystal structure of the receptor in the active state (PDB 5G53). All non-receptor components were removed, and missing residues added using MODELLER 9.23(121). Default protonation states of ionizable residues were used. The resulting structure was converted to MARTINI coarse-grained topology using the martinize.py script(122). The ELNeDyn elastic network(123) was used to constrain protein secondary and tertiary structures with a force constant of 500 kJ/mol/nm^2 and a cutoff of 1.5 nm. To optimize loop refinement of the model, a single copy was embedded in a 1-palmitoyl-2-oleoyl-sn-glycero-3-phosphocholine (POPC) bilayer using the insane.py script, solvated with MARTINI polarizable water, neutralized with 0.15 M NaCl, and a short MD (1.5 μs) run to equilibrate the loop regions. Subsequently, two monomers of the equilibrated $A_{2A}R$ were randomly rotated and placed at the center of a 13 nm × 13 nm × 11 nm (xyz) box, 3.5 nm apart, with their principal transmembrane axis aligned parallel to the z axis. The proteins were then embedded in a POPC bilayer using the insane.py script. Sodium and chloride ions were added to neutralize the system and obtain a concentration of 0.15 M NaCl. Total system size was typically in the range of 34,000 CG particles, with a 280:1 lipid:protein ratio. Ten independent copies were generated for each $A_{2A}R$ truncated variant.

v2.2 of the MARTINI coarse-grained force field(124) was used for the protein and water, and v2.0 was used for POPC. All coarse-grained simulations were carried out in GROMACS 2016(125) in the NPT ensemble (P = 1 atm, T = 310 K). The Bussi velocity rescaling thermostat was used for temperature control with a coupling constant of τ_t = 1.0 ps(126), while the Parrinello-

Rahman barostat(127) was used to control the pressure semi-isotropically with a coupling constant of τ_t = 12.0 ps and compressibility of 3 x 10^{-4} bar^{-1}. Reaction field electrostatics was used with Coulomb cut-off of 1.1 nm. Non-bonded Lennard-Jones interactions were treated with a cut-off of 1.1 nm. All simulations were run with a 15 fs timestep, updating neighbor lists every 10 steps. Cubic periodic boundary conditions along the x, y and z axes were used. Each simulation was run for 8 μs.

Atomistic MD Simulations

Three snapshots of symmetric dimers of $A_{2A}R$ for each respective truncated variant were randomly selected from the CG simulations as starting structures for backmapping. Coarse-grained systems were converted to atomistic resolution using the backward.py script(128). All simulations were run in Gromacs2019 in the *NPT* ensemble (P = 1 bar, T = 310 K) with all bonds restrained using the LINCS method(129). The Parrinello-Rahman barostat was used to control the pressure semi-isotropically with a coupling constant of τ_t = 1.0 ps and a compressibility of 4.5 x 10^{-5} bar^{-1}, while the Bussi velocity rescaling thermostat was used for temperature control with a coupling constant of τ_t = 0.1 ps. Proteins, lipids, and solvents were separately coupled to the thermostat. The CHARMM36 and TIP3P force fields(130, 131) were used to model all molecular interactions. Periodic boundary conditions were set in the x, y, and z directions. Particle mesh Ewald (PME) electrostatics was used with a cut-off of 1.0 nm. A 2-fs time step was used for all atomistic runs, and each simulation was run for 50 ns.

Analysis of Computational Results

All trajectories were post-processed using gromacs tools and in-house scripts. We ran a clustering analysis of all dimer frames from the CG simulations using Daura et. al.'s clustering algorithm(132) implemented in GROMACS, with an RMSD cutoff of 1.5 Å. (An interface was considered dimeric if the minimum center of mass distance between the protomers was less than 5 Å.) This method uses an RMSD cutoff to group all conformations with the largest number of neighbors into a cluster and eliminates these from the pool, then repeats the process until the pool is empty. We focused our analysis on the most populated cluster from each truncated variant. Electrostatic interactions in the dimer were calculated from CG systems with LOOS(133) using a distance cutoff of 5.0 Å.

Transmembrane helical tilt angles were also calculated in LOOS from CG simulations. Hydrogen bonds were calculated from AA simulations using the hydrogen bonds plugin in VMD(134), with a distance cutoff of 3.5 Å and an angle cutoff of 20º. Only C-terminal residues were included in hydrogen bond analysis. PyMOL(135) was used for molecular visualizations.

Assessing $A_{2A}R$ Oligomerization with Increasing Ionic Strength

Na_2HPO_4 and NaH_2PO_4 in the buffer make up an ionic strength of 0.15 M, to which NaCl was added to increase the ionic strength to 0.45 M and furthermore to 0.95 M. The $A_{2A}R$ variants were purified at 0.45 M ionic strength and then exchanged into buffers of different ionic strengths using a PD-10 desalting column prior to subjecting the samples to SEC. The buffer composition is detailed below.

Buffers	***Components***	***Conc. (mM)***	***Ionic Strength (mM)***
0.15 M Ionic Strength	**NaCl**	**0**	**0**
	NaH_2PO_4	4	4
	Na_2HPO_4	49	146
0.45 M Ionic Strength	**NaCl**	**300**	**300**
	NaH_2PO_4	4	4
	Na_2HPO_4	49	146
0.95 M Ionic Strength	**NaCl**	**800**	**800**
	NaH_2PO_4	4	4
	Na_2HPO_4	49	146

Table 1. *Calculations regarding composition of the buffers used in the experiments where salt concentrations are varied. Only NaCl concentration (in bold) is varied to achieve the different ionic strengths.*

Isolated C-Terminus Purification

Escherichia coli BL21 (DE3) cells were transfected with pET28a DNA plasmids containing the desired $A_{2A}R$ sequence with a 6x His tag attached for purification. Cells from glycerol stock were grown in 10 mL luria broth (LB, Sigma Aldrich, L3022) overnight at 37˚C and then used to inoculate 1 L of fresh LB and 10 μg/mL kanamycin (Fisher Scientific, BP906). Growth of cells were performed at 37°C, 200 rpm until optical density at $\lambda = 600$ nm reached 0.6–0.8. Expression was induced by incubation with 1 mM isopropyl-β-D-thiogalactoside (Fisher Bioreagents, BP175510) for 3 hrs.

Cells were harvested with centrifugation at 5000 rpm for 30 min. Harvested cells were resuspended in 25 mL Tris-HCl, pH = 7.4, 100 mM NaCl, 0.5 mM DTT, 0.1 mM EDTA with 1 Pierce protease inhibitor tablet (Thermo Scientific, A32965), 1 mM PMSF, 2 mg/mL lysozyme, 20 μg/mL DNase (Sigma, DN25) and 10 mM $MgCl_2$, and incubated on ice for 30 min. Samples were then incubated at 30ºC for 20 minutes, then flash frozen and thawed 3 times in LN_2. Samples were then centrifuged at 10,000 rpm for 10 min to remove cell debris. 1 mM PMSF was added again and the resulting supernatant was incubated while rotating for at least 4 hrs with Ni-NTA resin. The resin was loaded to a column and washed with 25 mL 20 mM sodium phosphate, pH = 7.0, 1 M NaCl, 20 mM imidazole, 0.5 mM DTT, 100 μM EDTA. Purified protein was eluted with 15 mL of 20 mM sodium phosphate, pH = 7.0, 0.5 mM DTT, 100 mM NaCl, 300 mM imidazole. The protein was concentrated to a volume of 2.5mL and was buffer exchanged into 20 mM ammonium acetate buffer, pH = 7.4, 100 mM NaCl using a GE PD-10 desalting column. Purity of sample was confirmed with SDS-PAGE and western blot.

Aggregation Assay to Assess $A_{2A}R$ C-Terminus Assembly

Absorbance was measured at 450 nm using a Shimadzu UV-1601 spectrophotometer with 120 μL sample size. Prior to reading, samples were incubated at 40°C for 5 minutes. Samples were vigorously pipetted to homogenize any precipitate before absorbance was measured. Protein concentration was 50 μM in a 20 mM ammonium acetate buffer (pH = 7.4).

Differential Scanning Fluorimetry (DSF)

DSF was conducted with a Bio-rad CFX90 real-time PCR machine. A starting temperature 20ºC was increased at a rate of 0.5ºC per 30 seconds to a final temperature of 85ºC. All samples contained 40 µL of 40 μM $A_{2A}R$ C-terminus, 9x SYPRO orange (ThermoFisher S6650), 200 mM NaCl, and 20 mM MES. Fluorescence was detected in real-time at 570 nm. All samples were conducted in triplicate.

Hydrophobicity and Charge Profile of C-Terminus

The hydrophobicity profile reported in **Fig. S4** was determined with ProtScale using method described by Kyte & Doolittle(136), window size of 3.

FUNDING AND ACKNOWLEDGMENTS

This material is based upon work supported by (1) the National Institute of General Medical Sciences of the National Institutes of Health under Award Number R35GM136411, (2) the National Institute of Mental Health of the National Institutes of Health under Small Business Innovation Research Award Number 1R43MH119906-01, and (3) the National Science Foundation under Award Number MCB-1714888 (E.S. and B.M.). The content is solely the responsibility of the authors and does not necessarily represent the official views of the National Institutes of Health. Many of the experiments were completed with the assistance from Rohan Katpally. The pITy expression vector and *S. cerevisiae* BJ5464 strain were generously provided by Prof. Anne Robinson's lab at Carnegie Mellon University. The X7 polymerase was a gift from Dr. Morten Nørholm, Novo Nordisk Foundation Center for Biosustainability, Technical University of Denmark. Computational time was provided through WVU Research Computing and XSEDE allocation no. TG-MCB130040.

REFERENCES

1. L. El-Asmar, *et al.*, Evidence for Negative Binding Cooperativity within CCR5-CCR2b Heterodimers. *Mol. Pharmacol.* **67**, 460–469 (2005).

2. V. Casadó-Anguera, *et al.*, Evidence for the heterotetrameric structure of the adenosine A2A–dopamine D2 receptor complex. *Biochem. Soc. Trans.* **44**, 595–600 (2016).

3. X. Guitart, *et al.*, Functional Selectivity of Allosteric Interactions within G Protein–Coupled Receptor Oligomers: The Dopamine D $_1$ -D $_3$ Receptor Heterotetramer. *Mol. Pharmacol.* **86**, 417–429 (2014).

4. K. Yoshioka, O. Saitoh, H. Nakata, Heteromeric association creates a P2Y-like adenosine receptor. *Proc. Natl. Acad. Sci.* **98**, 7617–7622 (2001).

5. S. Cristóvão-Ferreira, *et al.*, A1R–A2AR heteromers coupled to Gs and Gi/0 proteins modulate GABA transport into astrocytes. *Purinergic Signal.* **9**, 433–449 (2013).

6. A. Cordomí, G. Navarro, M. S. Aymerich, R. Franco, Structures for G-Protein-Coupled Receptor Tetramers in Complex with G Proteins. *Trends Biochem. Sci.* **40**, 548–551 (2015).

7. J. González-Maeso, *et al.*, Hallucinogens Recruit Specific Cortical 5-HT2A Receptor-Mediated Signaling Pathways to Affect Behavior. *Neuron* **53**, 439–452 (2007).

8. S. P. Lee, *et al.*, Dopamine D1 and D2 Receptor Co-activation Generates a Novel Phospholipase C-mediated Calcium Signal. *J. Biol. Chem.* **279**, 35671–35678 (2004).

9. A. J. Rashid, *et al.*, D1-D2 dopamine receptor heterooligomers with unique pharmacology are coupled to rapid activation of Gq/11 in the striatum. *Proc. Natl. Acad. Sci.* **104**, 654–659 (2007).

10. H. Liu, *et al.*, Heterodimerization of the kappa opioid receptor and neurotensin receptor 1 contributes to a novel β-arrestin-2–biased pathway. *Biochim. Biophys. Acta BBA - Mol. Cell Res.* **1863**, 2719–2738 (2016).

11. S. Hilairet, M. Bouaboula, D. Carrière, G. Le Fur, P. Casellas, Hypersensitization of the Orexin 1 Receptor by the CB1 Receptor: EVIDENCE FOR CROSS-TALK BLOCKED BY THE SPECIFIC CB1 ANTAGONIST, SR141716. *J. Biol. Chem.* **278**, 23731–23737 (2003).

12. R. Rozenfeld, L. A. Devi, Receptor heterodimerization leads to a switch in signaling: β-arrestin2-mediated ERK activation by μ-δ opioid receptor heterodimers. *FASEB J.* **21**, 2455–2465 (2007).

13. D. O. Borroto-Escuela, *et al.*, Galanin receptor-1 modulates 5-hydroxtryptamine-1A signaling via heterodimerization. *Biochem. Biophys. Res. Commun.* **393**, 767–772 (2010).

14. D. Ecke, *et al.*, Hetero-oligomerization of the P2Y11 receptor with the P2Y1 receptor controls the internalization and ligand selectivity of the P2Y11 receptor. *Biochem. J.* **409**, 107–116 (2008).

15. L. Stanasila, J.-B. Perez, H. Vogel, S. Cotecchia, Oligomerization of the α_{1a}- and α_{1b}-Adrenergic Receptor Subtypes: POTENTIAL IMPLICATIONS IN RECEPTOR INTERNALIZATION. *J. Biol. Chem.* **278**, 40239–40251 (2003).

16. O. Faklaris, *et al.*, Multicolor time-resolved Förster resonance energy transfer microscopy reveals the impact of GPCR oligomerization on internalization processes. *FASEB J.* **29**, 2235–2246 (2015).

17. S. Takeda, S. Kadowaki, T. Haga, H. Takaesu, S. Mitaku, Identification of G protein-coupled receptor genes from the human genome sequence. *FEBS Lett.* **520**, 97–101 (2002).

18. R. T. Dorsam, J. S. Gutkind, G-protein-coupled receptors and cancer. *Nat. Rev. Cancer* **7**, 79–94 (2007).

19. B. Farran, An update on the physiological and therapeutic relevance of GPCR oligomers. *Pharmacol. Res.* **117**, 303–327 (2017).

20. N. S. Schonenbach, S. Hussain, M. A. O'Malley, Structure and function of G protein-coupled receptor oligomers: implications for drug discovery: Studying GPCR Oligomer Function. *Wiley Interdiscip. Rev. Nanomed. Nanobiotechnol.* **7**, 408–427 (2015).

21. S. Ferré, *et al.*, G Protein–Coupled Receptor Oligomerization Revisited: Functional and Pharmacological Perspectives. *Pharmacol. Rev.* **66**, 413–434 (2014).

22. H. Bräuner-Osborne, P. Wellendorph, A. A. Jensen, "Structure, Pharmacology and Therapeutic Prospects of Family C G-Protein Coupled Receptors" in *Current Drug Targets*. (Bentham 2007), pp 169–184(16).

23. S. R. George, B. F. O'Dowd, S. P. Lee, G-Protein-coupled receptor oligomerization and its potential for drug discovery. *Nat. Rev. Drug Discov.* **1**, 808–820 (2002).

24. W. Song, A. L. Duncan, M. S. P. Sansom, "GPCR Oligomerisation Modulation by Conformational State and Lipid Interactions Revealed by MD Simulations and Markov Models" (Biophysics, 2020) https:/doi.org/10.1101/2020.06.24.168260 (July 22, 2020).

25. A. Ghosh, U. Sonavane, R. Joshi, Multiscale modelling to understand the self-assembly mechanism of human β2-adrenergic receptor in lipid bilayer. *Comput. Biol. Chem.* **48**, 29–39 (2014).

26. X. Periole, A. M. Knepp, T. P. Sakmar, S. J. Marrink, T. Huber, Structural Determinants of the Supramolecular Organization of G Protein-Coupled Receptors in Bilayers. *J. Am. Chem. Soc.* **134**, 10959–10965 (2012).

27. F. Fanelli, A. Felline, Dimerization and ligand binding affect the structure network of A2A adenosine receptor. *Biochim. Biophys. Acta BBA - Biomembr.* **1808**, 1256–1266 (2011).

28. W. Liu, *et al.*, Structural Basis for Allosteric Regulation of GPCRs by Sodium Ions. *Science* **337**, 232–236 (2012).

29. J. Huang, S. Chen, J. J. Zhang, X.-Y. Huang, Crystal structure of oligomeric β1-adrenergic G protein–coupled receptors in ligand-free basal state. *Nat. Struct. Mol. Biol.* **20**, 419–425 (2013).

30. A. Manglik, *et al.*, Crystal structure of the μ-opioid receptor bound to a morphinan antagonist. *Nature* **485**, 321–326 (2012).

31. T. S. Thorsen, R. Matt, W. I. Weis, B. K. Kobilka, Modified T4 Lysozyme Fusion Proteins Facilitate G Protein-Coupled Receptor Crystallogenesis. *Structure* **22**, 1657–1664 (2014).

32. D. Fotiadis, *et al.*, Structure of the rhodopsin dimer: a working model for G-protein-coupled receptors. *Curr. Opin. Struct. Biol.* **16**, 252–259 (2006).

33. D. Fotiadis, *et al.*, Atomic-force microscopy Rhodopsin dimers in native disc membranes. *Nature* **421**, 127–128 (2003).

34. Y. Liang, *et al.*, Organization of the G Protein-coupled Receptors Rhodopsin and Opsin in Native Membranes. *J. Biol. Chem.* **278**, 21655–21662 (2003).

35. L. Xue, *et al.*, Major ligand-induced rearrangement of the heptahelical domain interface in a GPCR dimer. *Nat. Chem. Biol.* **11**, 134–140 (2015).

36. P. M. Dijkman, *et al.*, Dynamic tuneable G protein-coupled receptor monomer-dimer populations. *Nat. Commun.* **9**, 1710 (2018).

37. S. Asakura, F. Oosawa, Interaction between particles suspended in solutions of macromolecules. *J. Polym. Sci.* **33**, 183–192 (1958).

38. A. G. Yodh, *et al.*, Entropically driven self–assembly and interaction in suspension. *Philos. Trans. R. Soc. Lond. Ser. Math. Phys. Eng. Sci.* **359**, 921–937 (2001).

39. D. Marenduzzo, K. Finan, P. R. Cook, The depletion attraction: an underappreciated force driving cellular organization. *J. Cell Biol.* **175**, 681–686 (2006).

40. S. Milles, N. Salvi, M. Blackledge, M. R. Jensen, Characterization of intrinsically disordered proteins and their dynamic complexes: From in vitro to cell-like environments. *Prog. Nucl. Magn. Reson. Spectrosc.* **109**, 79–100 (2018).

41. B. I. M. Wicky, S. L. Shammas, J. Clarke, Affinity of IDPs to their targets is modulated by ion-specific changes in kinetics and residual structure. *Proc. Natl. Acad. Sci.* **114**, 9882–9887 (2017).

42. Cs. Szasz, *et al.*, Protein Disorder Prevails under Crowded Conditions. *Biochemistry* **50**, 5834–5844 (2011).

43. D. P. Goldenberg, B. Argyle, Minimal Effects of Macromolecular Crowding on an Intrinsically Disordered Protein: A Small-Angle Neutron Scattering Study. *Biophys. J.* **106**, 905–914 (2014).

44. S. Qin, H.-X. Zhou, Effects of Macromolecular Crowding on the Conformational Ensembles of Disordered Proteins. *J. Phys. Chem. Lett.* **4**, 3429–3434 (2013).

45. E. A. Cino, M. Karttunen, W.-Y. Choy, Effects of Molecular Crowding on the Dynamics of Intrinsically Disordered Proteins. *PLoS ONE* **7**, e49876 (2012).

46. A. Soranno, *et al.*, Single-molecule spectroscopy reveals polymer effects of disordered proteins in crowded environments. *Proc. Natl. Acad. Sci.* **111**, 4874–4879 (2014).

47. F. Zosel, A. Soranno, K. J. Buholzer, D. Nettels, B. Schuler, Depletion interactions modulate the binding between disordered proteins in crowded environments. *Proc. Natl. Acad. Sci.* **117**, 13480–13489 (2020).

48. N. F. A. van der Vegt, D. Nayar, The Hydrophobic Effect and the Role of Cosolvents. *J. Phys. Chem. B* **121**, 9986–9998 (2017).

49. W. Kunz, J. Henle, B. W. Ninham, 'Zur Lehre von der Wirkung der Salze' (about the science of the effect of salts): Franz Hofmeister's historical papers. *Curr. Opin. Colloid Interface Sci.* **9**, 19–37 (2004).

50. L. Tovo-Rodrigues, A. Roux, M. H. Hutz, L. A. Rohde, A. S. Woods, Functional characterization of G-protein-coupled receptors: A bioinformatics approach. *Neuroscience* **277**, 764–779 (2014).

51. V.-P. Jaakola, J. Prilusky, J. L. Sussman, A. Goldman, G protein-coupled receptors show unusual patterns of intrinsic unfolding. *Protein Eng. Des. Sel.* **18**, 103–110 (2005).

52. J. Garcıa-Nafrıa, Y. Lee, X. Bai, B. Carpenter, C. G. Tate, Cryo-EM structure of the adenosine A2A receptor coupled to an engineered heterotrimeric G protein. *eLife* **7**, e35946 (2018).

53. B. Sun, *et al.*, Crystal structure of the adenosine A $_{2A}$ receptor bound to an antagonist reveals a potential allosteric pocket. *Proc. Natl. Acad. Sci.* **114**, 2066–2071 (2017).

54. G. Lebon, *et al.*, Agonist-bound adenosine A2A receptor structures reveal common features of GPCR activation. *Nature* **474**, 521–525 (2011).

804 55. F. Xu, *et al.*, Structure of an Agonist-Bound Human A2A Adenosine Receptor. **332**, 7
805 (2011).

806 56. A. S. Doré, *et al.*, Structure of the Adenosine A2A Receptor in Complex with ZM241385
807 and the Xanthines XAC and Caffeine. *Structure* **19**, 1283–1293 (2011).

808 57. V.-P. Jaakola, *et al.*, The 2.6 Angstrom Crystal Structure of a Human A2A Adenosine
809 Receptor Bound to an Antagonist. *Science* **322**, 1211–1217 (2008).

810 58. B. Carpenter, R. Nehmé, T. Warne, A. G. W. Leslie, C. G. Tate, Structure of the
811 adenosine A2A receptor bound to an engineered G protein. *Nature* **536**, 104–107 (2016).

812 59. T. Hino, *et al.*, G-protein-coupled receptor inactivation by an allosteric inverse-agonist
813 antibody. *Nature* **482**, 237–240 (2012).

814 60. K. S. Koretz, C. McGraw, A. S. Robinson, Characterization of A2AR and G Protein
815 Coupling by Surface Plasmon Resonance. *Biophys. J.* **118**, 162a (2020).

816 61. G. Navarro, *et al.*, Cross-communication between Gi and Gs in a G-protein-coupled
817 receptor heterotetramer guided by a receptor C-terminal domain. *BMC Biol.* **16** (2018).

818 62. A. Jain, C. McGraw, A. Robinson, The Adenosine A1 and A2A Receptor C-termini are
819 Necessary for Activation but not the Specificity of Downstream Signaling
820 https:/doi.org/10.22541/au.158532015.55605148 (November 24, 2020).

821 63. N. S. Schonenbach, M. D. Rieth, S. Han, M. A. O'Malley, Adenosine A2a receptors form
822 distinct oligomers in protein detergent complexes. *FEBS Lett.* **590**, 3295–3306 (2016).

823 64. S. Cvejic, L. A. Devi, Dimerization of the δ Opioid Receptor: IMPLICATION FOR A
824 ROLE IN RECEPTOR INTERNALIZATION. *J. Biol. Chem.* **272**, 26959–26964 (1997).

825 65. J. Burgueño, *et al.*, The Adenosine A $_{2A}$ Receptor Interacts with the Actin-binding
826 Protein α-Actinin. *J. Biol. Chem.* **278**, 37545–37552 (2003).

827 66. F. Ciruela, *et al.*, Combining Mass Spectrometry and Pull-Down Techniques for the
828 Study of Receptor Heteromerization. Direct Epitope−Epitope Electrostatic Interactions
829 between Adenosine A $_{2A}$ and Dopamine D $_{2}$ Receptors. *Anal. Chem.* **76**, 5354–5363
830 (2004).

831 67. P. K. Grover, R. L. Ryall, Critical Appraisal of Salting-Out and Its Implications for
832 Chemical and Biological Sciences. *Chem. Rev.* **105**, 1–10 (2005).

833 68. A. S. Thomas, A. H. Elcock, Molecular Dynamics Simulations of Hydrophobic
834 Associations in Aqueous Salt Solutions Indicate a Connection between Water Hydrogen
835 Bonding and the Hofmeister Effect. *J. Am. Chem. Soc.* **129**, 14887–14898 (2007).

836 69. G. Graziano, Hydrophobic interaction of two large plates: An analysis of salting-
837 in/salting-out effects. *Chem. Phys. Lett.* **491**, 54–58 (2010).

70. R. Zangi, M. Hagen, B. J. Berne, Effect of Ions on the Hydrophobic Interaction between Two Plates. *J. Am. Chem. Soc.* **129**, 4678–4686 (2007).

71. J. Heyda, *et al.*, Guanidinium can both Cause and Prevent the Hydrophobic Collapse of Biomacromolecules. *J. Am. Chem. Soc.* **139**, 863–870 (2017).

72. R. L. Baldwin, How Hofmeister ion interactions affect protein stability. *Biophys. J.* **71**, 2056–2063 (1996).

73. T. A. Larsen, A. J. Olson, D. S. Goodsell, Morphology of protein–protein interfaces. *Structure* **6**, 421–427 (1998).

74. C.-J. Tsai, R. Nussinov, Hydrophobic folding units at protein-protein interfaces: Implications to protein folding and to protein-protein association. *Protein Sci.* **6**, 1426–1437 (1997).

75. C.-J. Tsai, S. L. Lin, H. J. Wolfson, R. Nussinov, Studies of protein-protein interfaces: A statistical analysis of the hydrophobic effect: Protein-protein interfaces: The hydrophobic effect. *Protein Sci.* **6**, 53–64 (1997).

76. E. De Filippo, *et al.*, Role of extracellular cysteine residues in the adenosine A2A receptor. *Purinergic Signal.* **12**, 313–329 (2016).

77. A. N. Naranjo, *et al.*, Conserved disulfide bond is not essential for the adenosine A2A receptor: Extracellular cysteines influence receptor distribution within the cell and ligand-binding recognition. *Biochim. Biophys. Acta BBA - Biomembr.* **1848**, 603–614 (2015).

78. M. A. O'Malley, A. N. Naranjo, T. Lazarova, A. S. Robinson, Analysis of Adenosine A $_2$ a Receptor Stability: Effects of Ligands and Disulfide Bonds. *Biochemistry* **49**, 9181–9189 (2010).

79. L. Gama, S. G. Wilt, G. E. Breitwieser, Heterodimerization of Calcium Sensing Receptors with Metabotropic Glutamate Receptors in Neurons. *J. Biol. Chem.* **276**, 39053–39059 (2001).

80. C. Romano, W.-L. Yang, K. L. O'Malley, Metabotropic Glutamate Receptor 5 Is a Disulfide-linked Dimer. *J. Biol. Chem.* **271**, 28612–28616 (1996).

81. F.-Y. Zeng, J. Wess, Identification and Molecular Characterization of m3 Muscarinic Receptor Dimers. *J. Biol. Chem.* **274**, 19487–19497 (1999).

82. X. Zhu, J. Wess, Truncated V2 Vasopressin Receptors as Negative Regulators of Wild-Type V2 Receptor Function. *Biochemistry* **37**, 15773–15784 (1998).

83. M. Berthouze, *et al.*, Two transmembrane Cys residues are involved in 5-HT4 receptor dimerization. *Biochem. Biophys. Res. Commun.* **356**, 642–647 (2007).

84. S. P. Lee, Z. Xie, B. F. O'Dowd, Oligomerization of Dopamine and Serotonin Receptors. *Neuropsychopharmacol.* **23**, S32–S40 (2000).

85. W. Guo, *et al.*, Dopamine D2 receptors form higher order oligomers at physiological expression levels. *EMBO J.* **27**, 2293–2304 (2008).

86. M. J. Saaranen, L. W. Ruddock, Disulfide Bond Formation in the Cytoplasm. *Antioxid. Redox Signal.* **19**, 46–53 (2013).

87. J. K. Locker, G. Griffiths, An Unconventional Role for Cytoplasmic Disulfide Bonds in Vaccinia Virus Proteins. *J. Cell Biol.* **144**, 267–279 (1999).

88. J. R. Gaut, L. M. Hendershot, The modification and assembly of proteins in the endoplasmic reticulum. *Curr. Opin. Cell Biol.* **5**, 589–595 (1993).

89. C. Hwang, A. Sinskey, H. Lodish, Oxidized redox state of glutathione in the endoplasmic reticulum. *Science* **257**, 1496–1502 (1992).

90. A. Helenius, T. Marquardt, I. Braakman, The endoplasmic reticulum as a protein-folding compartment. *Trends Cell Biol.* **2**, 227–231 (1992).

91. T. E. Creighton, D. A. Hillson, R. B. Freedman, Catalysis by protein-disulphide isomerase of the unfolding and refolding of proteins with disulphide bonds. *J. Mol. Biol.* **142**, 43–62 (1980).

92. G. Pándy-Szekeres, *et al.*, GPCRdb in 2018: adding GPCR structure models and ligands. *Nucleic Acids Res.* **46**, D440–D446 (2018).

93. R. S. Kasai, S. V. Ito, R. M. Awane, T. K. Fujiwara, A. Kusumi, The Class-A GPCR Dopamine D2 Receptor Forms Transient Dimers Stabilized by Agonists: Detection by Single-Molecule Tracking. *Cell Biochem. Biophys.* **76**, 29–37 (2018).

94. A. Tabor, *et al.*, Visualization and ligand-induced modulation of dopamine receptor dimerization at the single molecule level. *Sci. Rep.* **6** (2016).

95. J. Möller, *et al.*, Single-molecule analysis reveals agonist-specific dimer formation of μ-opioid receptors. *Nat. Chem. Biol.* **16**, 946–954 (2020).

96. J.-P. Vilardaga, *et al.*, Conformational cross-talk between α2A-adrenergic and μ-opioid receptors controls cell signaling. *Nat. Chem. Biol.* **4**, 126–131 (2008).

97. U. Golebiewska, J. M. Johnston, L. Devi, M. Filizola, S. Scarlata, Differential Response to Morphine of the Oligomeric State of μ-Opioid in the Presence of δ-Opioid Receptors. *Biochemistry* **50**, 2829–2837 (2011).

98. S. Armando, *et al.*, The chemokine CXC4 and CC2 receptors form homo- and heterooligomers that can engage their signaling G-protein effectors and βarrestin. *FASEB J.* **28**, 4509–4523 (2014).

99. A. M. Bagher, R. B. Laprairie, J. T. Toguri, M. E. M. Kelly, E. M. Denovan-Wright, Bidirectional allosteric interactions between cannabinoid receptor 1 (CB1) and dopamine receptor 2 long (D2L) heterotetramers. *Eur. J. Pharmacol.* **813**, 66–83 (2017).

100. G. Navarro, *et al.*, Quaternary structure of a G-protein-coupled receptor heterotetramer in complex with Gi and Gs. *BMC Biol.* **14** (2016).

101. G. Navarro, *et al.*, Evidence for functional pre-coupled complexes of receptor heteromers and adenylyl cyclase. *Nat. Commun.* **9** (2018).

102. A. Cordomí, G. Navarro, L. Pardo, R. Franco, "Structure of G-protein-coupled receptor heteromers" in *GPCRs*, (Elsevier, 2020), pp. 109–119.

103. P.-A. Vidi, J. Chen, J. M. K. Irudayaraj, V. J. Watts, Adenosine A $_{2A}$ receptors assemble into higher-order oligomers at the plasma membrane. *FEBS Lett.* **582**, 3985–3990 (2008).

104. M. T. Eddy, *et al.*, Allosteric Coupling of Drug Binding and Intracellular Signaling in the A2A. *Cell* **172,** 68–80.e12 (2018).

105. L. Sušac, M. T. Eddy, T. Didenko, R. C. Stevens, K. Wüthrich, A $_{2A}$ adenosine receptor functional states characterized by ^{19} F-NMR. *Proc. Natl. Acad. Sci.*, **115**, 12733–12738 (2018).

106. R. S. Prosser, L. Ye, A. Pandey, A. Orazietti, Activation processes in ligand-activated G protein-coupled receptors: A case study of the adenosine A $_{2A}$ receptor. *BioEssays* **39**, 1700072 (2017).

107. L. Ye, N. Van Eps, M. Zimmer, O. P. Ernst, R. Scott Prosser, Activation of the A2A adenosine G-protein-coupled receptor by conformational selection. *Nature* **533**, 265–268 (2016).

108. T. Mirzadegan, G. Benko, S. Filipek, K. Palczewski, Sequence Analyses of G-Protein-Coupled Receptors: Similarities to Rhodopsin. *Biochem.* **42**, 9.

109. V. V. Gurevich, E. V. Gurevich, How and why do GPCRs dimerize? *Trends Pharmacol. Sci.* **29**, 234–240 (2008).

110. R. N. Parekh, M. R. Shaw, K. D. Wittrup, An Integrating Vector for Tunable, High Copy, Stable Integration into the Dispersed Ty δ Sites of Saccharomyces cerevisiae. *Biotechnol. Prog.* **12**, 16–21 (1996).

111. M. A. O'Malley, *et al.*, Progress toward heterologous expression of active G-protein-coupled receptors in *Saccharomyces cerevisiae* : Linking cellular stress response with translocation and trafficking. *Protein Sci.* **18**, 2356–2370 (2009).

112. J. M. Clements, G. H. Catlin, M. J. Price, R. M. Edwards, Secretion of human epidermal growth factor from Saccharomyces cerevisiae using synthetic leader sequences. *Gene* **106**, 267–271 (1991).

941 113. R. N. Parekh, K. J. Forrester, D. Wittrup, Multicopy Overexpression of Bovine
942 Pancreatic Trypsin Inhibitor Saturates the Protein Folding and Secretory Capacity of
943 Saccharomyces cerevisiae. *Protein Expr. Purif.* **6**, 537–545 (1995).

944 114. A. Bryksin, I. Matsumura, Overlap extension PCR cloning: a simple and reliable way to
945 create recombinant plasmids. *BioTechniques* **48**, 463–465 (2010).

946 115. M. H. Nørholm, A mutant Pfu DNA polymerase designed for advanced uracil-excision
947 DNA engineering. *BMC Biotechnol.* **10**, 21 (2010).

948 116. H. H. Nour-Eldin, B. G. Hansen, M. H. H. Nørholm, J. K. Jensen, B. A. Halkier,
949 Advancing uracil-excision based cloning towards an ideal technique for cloning PCR
950 fragments. *Nucleic Acids Res.* **34**, e122–e122 (2006).

951 117. R. D. Gietz, "Yeast Transformation by the LiAc/SS Carrier DNA/PEG Method" in *Yeast*
952 *Protocols*, Methods in Molecular Biology., W. Xiao, Ed. (Springer New York, 2014), pp.
953 33–44.

954 118. R. T. Niebauer, A. S. Robinson, Exceptional total and functional yields of the human
955 adenosine (A2a) receptor expressed in the yeast Saccharomyces cerevisiae. *Protein Expr.*
956 *Purif.* **46**, 204–211 (2006).

957 119. M. A. O'Malley, T. Lazarova, Z. T. Britton, A. S. Robinson, High-level expression in
958 Saccharomyces cerevisiae enables isolation and spectroscopic characterization of
959 functional human adenosine A2a receptor. *J. Struct. Biol.* **159**, 166–178 (2007).

960 120. H. M. Weiß, R. Grisshammer, Purification and characterization of the human adenosine
961 A2a receptor functionally expressed in Escherichia coli: Purification and characterization
962 of A2a receptor. *Eur. J. Biochem.* **269**, 82–92 (2002).

963 121. N. Eswar, *et al.*, Comparative Protein Structure Modeling Using Modeller. *Curr. Protoc.*
964 *Bioinforma.* **15**, 5.6.1-5.6.30 (2006).

965 122. D. H. de Jong, *et al.*, Improved Parameters for the Martini Coarse-Grained Protein Force
966 Field. *J. Chem. Theory Comput.* **9**, 687–697 (2013).

967 123. X. Periole, M. Cavalli, S.-J. Marrink, M. A. Ceruso, Combining an Elastic Network With
968 a Coarse-Grained Molecular Force Field: Structure, Dynamics, and Intermolecular
969 Recognition. *J. Chem. Theory Comput.* **5**, 2531–2543 (2009).

970 124. L. Monticelli, *et al.*, The MARTINI Coarse-Grained Force Field: Extension to Proteins.
971 *J. Chem. Theory Comput.* **4**, 819–834 (2008).

972 125. M. J. Abraham, *et al.*, GROMACS: High performance molecular simulations through
973 multi-level parallelism from laptops to supercomputers. *SoftwareX* **1–2**, 19–25 (2015).

974 126. G. Bussi, D. Donadio, M. Parrinello, Canonical sampling through velocity rescaling. *J.*
975 *Chem. Phys.* **126**, 014101 (2007).

127. R. Martoňák, A. Laio, M. Parrinello, Predicting Crystal Structures: The Parrinello-Rahman Method Revisited. *Phys. Rev. Lett.* **90** (2003).

128. T. A. Wassenaar, K. Pluhackova, R. A. Böckmann, S. J. Marrink, D. P. Tieleman, Going Backward: A Flexible Geometric Approach to Reverse Transformation from Coarse Grained to Atomistic Models. *J. Chem. Theory Comput.* **10**, 676–690 (2014).

129. B. Hess, H. Bekker, H. J. C. Berendsen, J. G. E. M. Fraaije, LINCS: A linear constraint solver for molecular simulations. *J. Comput. Chem.* **18**, 1463–1472 (1997).

130. R. B. Best, *et al.*, Optimization of the Additive CHARMM All-Atom Protein Force Field Targeting Improved Sampling of the Backbone ϕ, ψ and Side-Chain χ_1 and χ_2 Dihedral Angles. *J. Chem. Theory Comput.* **8**, 3257–3273 (2012).

131. W. L. Jorgensen, J. Chandrasekhar, J. D. Madura, R. W. Impey, M. L. Klein, Comparison of simple potential functions for simulating liquid water. *J. Chem. Phys.* **79**, 926–935 (1983).

132. X. Daura, *et al.*, Peptide Folding: When Simulation Meets Experiment. *Angew. Chem. Int. Ed.* **38**, 236–240 (1999).

133. T. D. Romo, A. Grossfield, LOOS: An extensible platform for the structural analysis of simulations in *2009 Annual International Conference of the IEEE Engineering in Medicine and Biology Society*, (IEEE, 2009), pp. 2332–2335.

134. W. Humphrey, A. Dalke, K. Schulten, VMD: Visual Molecular Dynamics. *J. Mol. Graph.* **14**, 33–38 (1996).

135. *The PyMOL Molecular Graphics System, Version 2.0 Schrödinger, LLC.*

136. J. Kyte, R. F. Doolittle, A simple method for displaying the hydropathic character of a protein. *J. Mol. Biol.* **157**, 105–132 (1982).